Optical multi-sites of Nd^{3+}-doped $CaMoO_4$ induced by Nb^{5+} charge compensator

2006 J. Phys.: Condens. Matter 18 7883

(http://iopscience.iop.org/0953-8984/18/34/003)

INSTITUTE OF PHYSICS PUBLISHING JOURNAL OF PHYSICS: CONDENSED MATTER

J. Phys.: Condens. Matter **18** (2006) 7883–7892 doi:10.1088/0953-8984/18/34/003

Optical multi-sites of Nd^{3+}-doped $CaMoO_4$ induced by Nb^{5+} charge compensator

L H C Andrade[1], M Siu Li[2], Y Guyot[3], A Brenier[3] and G Boulon[3]

[1] Universidade Estadual de Mato Grosso do Sul, Curso de Física, CP 351 CEP: 79804-970, Dourados, MS, Brazil
[2] Instituto de Física de São Carlos, Departamento de Física e Ciência dos Materiais, Universidade de São Paulo, CP 369, CEP 13560-970, São Carlos, SP, Brazil
[3] Laboratoire de Physico-Chimie des Matériaux Luminescents, Université Claude Bernard Lyon 1, UMR 5620 CNRS, 69622, Villeurbanne, France

E-mail: luis_hca@yahoo.com

Received 4 January 2006, in final form 8 July 2006
Published 7 August 2006
Online at stacks.iop.org/JPhysCM/18/7883

Abstract

Site-selective laser excitation and luminescence measurements at 15 K of $CaMoO_4$ single crystal doped with Nd^{3+} and co-doped with Nb^{5+} charge compensator have been investigated in the spectral region of laser interest involving the $^4F_{3/2} \rightarrow {}^4I_{11/2}$ transition. A larger than expected number of Nd^{3+} sites was found and a model to explain this result is presented. A partial diagram of $^4F_{3/2}$ and $^4I_{11/2}$ levels was constructed from the acquired data and their features are discussed.

1. Introduction

Nd^{3+} multi-site (non-equivalent centres) laser materials can be easily excited by a semiconductor diode laser because they generally have intense and large absorption bands at about 810 and 795 nm. This feature gives these materials a large advantage over high ordered laser materials like Nd:YAG or Nd:YLF, which have small optical absorption bandwidths and demand a precise wavelength control through temperature adjustment in the junction of the diode laser and the crystal. This adjustment requires a lot of energy and leads to a decrease of the efficiency of the lasing system [1]. Although crystals with disordered structures have demonstrated that they usually present broadening of both the absorption and emission bands, which is certainly convenient to avoid precise wavelength control, they also exhibit a decrease in the stimulated emission cross-section of rare earth ions and in the laser performance. Thus a compromise between broad absorption and emission bands, like in Nd:$CaWO_4$, and narrow but more intense corresponding bands, like in Nd:YAG, is required to match available pumping sources and have a better laser performance [2, 3].

Materials like $NaGd(WO_4)_2$, $KGd(WO_4)_2$, $CaWO_4$ and $KY(WO_4)_2$, from the scheelite family and with space group $I4_1/a$, have demonstrated desirable laser features [1] when doped with Nd^{3+}. Another material of the same family that has been known for four decades [4, 5] as a potential host for rare earth ions is $CaMoO_4$, but its laser properties from the standpoint of dopant and co-dopant accommodation in the crystal lattice have been only poorly investigated.

Most oxide laser materials where Nd^{3+} enters replacing a divalent cation must be co-doped with a charge compensator element in order to ensure the lattice electroneutrality and to increase the efficiency of dopant incorporation. This association, called 'heterovalent isomorphism', leads the formation of several multi-sites due to diverse possible accommodations of the charge compensator and activator ions [6, 7]. Such is the case of $CaMoO_4$ doped with Nd^{3+} and co-doped with the charge compensator Nb^{5+}, whose laser performance and emission properties have been reported as comparable to Nd:YAG by other authors [3–5].

Knowledge of the location of the active ions is important in predicting the laser properties of the material because the laser action is produced only when the active ions are located at specific crystal sites [8]. In this work, site-selective laser excitation and fluorescence (emission) measurements were performed to map and characterize the different non-equivalent Nd^{3+} sites in $CaMoO_4$ single crystal doped with Nd^{3+} and co-doped with Nb^{5+}, hereafter referred to as Nd, Nb:$CaMoO_4$, explaining the origin of the broad absorption and emission bands observed in previous work [3].

2. Thermochemistry and crystal growth

The synthesis of the raw material was carried out by solid state reaction using powders of optipure $CaCO_3$ (Merck), 99.95% MoO_3 (Alfa Aesar), 99.99% Nd_2O_3 (Merck) and 99.95% Nb_2O_5 (Merck). First, $CaCO_3$ and MoO_3 in 1:1 molar ratio were reacted at 800 °C for 10 h. Then, Nd_2O_3 and Nb_2O_5 in 1:1 molar ratio were reacted at 1150 °C for 12 h. The resulting powders in each case were weighed and mixed in the molar ratio $(1-x)$:x of $CaMoO_4$:$NdNbO_4$ with $x = 0.040$. Finally, each mixture was combined with a binder to form ceramic pastes that were shaped into cylindrical preforms. Single-crystal minirods were grown from these preforms without seeding by a floating zone-like technique, described elsewhere [3, 9].

Typical dimensions of the preforms were about 1.0 mm diameter and at least 20 mm length. The pulling velocity was 1.0 mm min^{-1} and the final diameter of each as-grown single-crystal minirod was about 0.8 mm. Thermal annealing at 1000 °C for 18 h was performed on each crystal to decrease the residual mechanical stress. The final Nd^{3+} concentration estimated from the lattice structure data and EDX measurements is $N = 1.175 \times 10^{20}$ ions cm^{-3}. Samples for study were obtained after polishing of the surfaces parallel and perpendicular to the growth axis of each minirod.

3. Characterization methods

All spectroscopic measurements were carried out with the samples glued with silver paint at the cold finger of cryostat coupled with a closed circuit helium refrigeration system (SMC–TBT–air liquid) by cooling the samples down to 15 K, a temperature at which only the lowest Stark component of the absorbing level $^4I_{9/2}$ and of the emitting level $^4F_{3/2}$ are populated.

Laser excitation was provided by radiation shifted from a hydrogen Raman cell excited by a dye laser (Quantel Datachrom 5000, DCM) that was pumped by a pulsed second harmonic of a Nd:YAG laser (Quantel YAG 581) (10 Hz, 10 ns). The excitation beam was tuned in the near infrared (IR) region from 850 to 890 nm with a linewidth of 0.2 cm^{-1} and energy of 0.5 mJ.

The detected IR signal was processed by a boxcar integrator (Stanford Research SR250) and analysed by a digital oscilloscope (Lecroy 9400) to record the excitation and emission spectra.

The non-selective excitation spectrum of the two $^4F_{3/2}$ Stark levels R_1 and R_2, labelled here $^4F_{3/2}$ (R_1, R_2), was acquired by monitoring the whole IR emission intensity with a room-temperature Ge detector behind a long pass filter (DJ1160). In order to refine this spectrum, site-selective excitation spectra of the respective emission signal were obtained by placing a monochromator (Jobin Yvon HRS1, grating of 600 grooves mm^{-1}, blazed at 1 μm) between the sample and a fast ($\sim$0.5 μs North Coast) germanium detector cooled by liquid nitrogen. This procedure was performed by scanning the excitation spectra for several wavelengths selected with small steps in the $^4F_{3/2}(R_1) \rightarrow {}^4I_{11/2}$ transition around 1.05 μm. Thus each component line of $^4I_{9/2}(Z_1) \rightarrow {}^4F_{3/2}(R_1)$ was coupled the another respective component line of $^4I_{9/2}(Z_1) \rightarrow {}^4F_{3/2}(R_2)$. This procedure allows verifying the number of different sites present in the samples and their Starks levels $^4F_{3/2}$ (R_1 and R_2). However, because some excitation bands in the $^4F_{3/2}(R_1)$ overlap each other, some site-selective excitation spectra present more than two excitation lines.

The site-selective luminescence spectrum of the $^4F_{3/2} \rightarrow {}^4I_{11/2}$ transition was also measured by scanning the laser excitation at $^4F_{3/2}(R_1)$ with a step of 2.5 Å and recording the emission spectra related to each excitation. Thus we could confirm each of the six Stark components (Y_1, Y_2, ... and Y_6) related to the $^4I_{11/2}$ level associated with each Nd^{3+} site. This procedure also permitted us to confirm the existence of another site detected from site-selective laser excitation.

The ground levels $^4I_{9/2}$ and $^4I_{11/2}$ are split into five and six Starks sublevels, respectively, and they are labelled here as $^4I_{9/2}$ (Z_1, Z_2, ..., Z_5) and $^4I_{11/2}$ (Y_1, Y_2, ..., Y_6). Meanwhile, the first excited state $^4F_{3/2}$ splits into only two Stark sublevels R_1 and R_2, labelled here $^4F_{3/2}(R_1, R_2)$.

4. Results and analysis

Figure 1 presents the full excitation spectrum (non-selective excitation spectrum) at 15 K of a Nd, Nb:$CaMoO_4$ single-crystal minirod. It was obtained by recording the whole IR intensity and avoiding the site selection related to the transition from $^4I_{9/2}(Z_1)$ to $^4F_{3/2}(R_1)$ and $^4F_{3/2}(R_2)$. Under these experimental conditions, the excitation spectrum is similar to the absorption spectrum, but it has the advantage of better resolution because of the use of a dye Raman shift tunable laser [6]. This full excitation spectrum shows at least four sharp peaks for the $^4I_{9/2}(Z_1) \rightarrow {}^4F_{3/2}(R_1)$ transition, which can be attributed initially to at least four different sites of Nd^{3+} in Nd, Nb:$CaMoO_4$. However, it can be noted that some peaks of $^4I_{9/2}(Z_1) \rightarrow {}^4F_{3/2}(R_1)$ seem not completely resolved; therefore there exists some missed band above, meaning other sites inside this region that can be resolved by the site-selective laser excitation experiment. It can be noted also that the band corresponding to the $^4I_{9/2}(Z_1) \rightarrow {}^4F_{3/2}(R_2)$ transition is broader than that of the $^4I_{9/2}(Z_1) \rightarrow {}^4F_{3/2}(R_1)$ transition. Therefore, site-selective laser excitation into the $^4I_{9/2}(Z_1) \rightarrow {}^4F_{3/2}(R_1)$ absorption band is more appropriate than exciting the $^4F_{3/2}(R_2)$ level in order to obtain the emission spectrum of each Nd^{3+} site [6, 7]. The splittings of separate Stark components in $^4F_{3/2}(R_1)$ and $^4F_{3/2}(R_2)$ of each Nd^{3+} site were identified using site-selective laser excitation and monitoring the emission intensity. Each one of these pairs of $^4I_{9/2}(Z_1) \rightarrow {}^4F_{3/2}(R_{1,2})$ has a characteristic emission spectrum composed of six emission lines. Most of them present more than two bands for the $^4I_{9/2}(Z_1) \rightarrow {}^4F_{3/2}(R_{1,2})$ transition, and when this situation was observed, there were more than six lines around 1.05 μm. This situation means that two or more sites have been simultaneously excited. Sometimes only two Stark components $^4I_{9/2}(Z_1) \rightarrow {}^4F_{3/2}(R_{1,2})$ and six peaks around

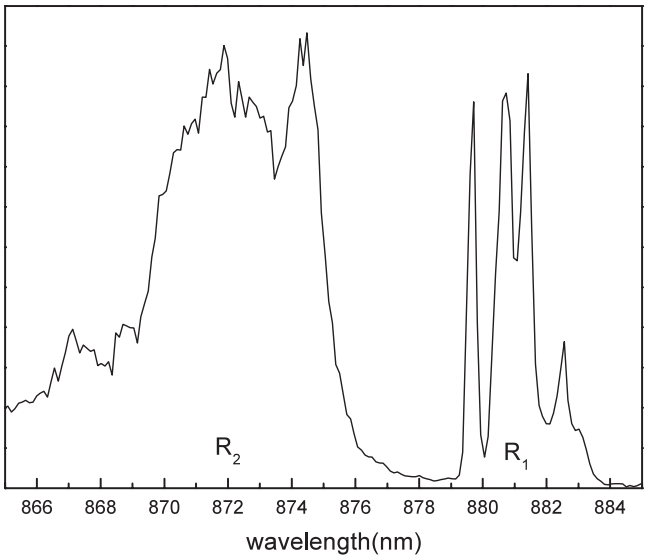

Figure 1. Excitation spectrum at 10 K of $NdNbO_4$-doped $CaMoO_4$ in the region of $^4F_{3/2}$ (R_1 and R_2 levels).

1.05 μm are present, meaning that only one site was excited. Different kinds of defect inside the crystal create local variations around the position of Nd^{3+} and Nd^{3+}–Nb^{5+} pairs, so these defects change the crystal field around the Nd^{3+} ions and appear in site-selective laser excitation spectra as a broadening in the spectra or some broad bands above the peaks. Figure 2 present examples of emission (excitation) spectra recorded in this way along with the full excitation spectrum used for comparison when two excitation lines were observed. The peak positions of $^4F_{3/2}(R_1)$ and $^4F_{3/2}(R_2)$ in this full excitation spectrum are indicated with the labels α β, ε, ξ, ζ, and δ. The small peak at 874.6 nm that appears above the excitation band of ξ and ε $^4F_{3/2}(R_2)$ Stark level corresponds to a new site labelled as γ and its second $^4F_{3/2}(R_1)$ Stark most probable position was found by site-selective emission experiment.

Although figure 1 obtained by the non-selective excitation experimental procedure has identified four sites, the selective excitation spectra shown in figure 2 permitted us to refine and resolve this spectrum and identify some missing bands above $^4I_{9/2}(Z_1) \rightarrow {}^4F_{3/2}(R_{1,2})$ transition level. However, some sites still appear overlapped with others, like sites δ and γ, due to defects around the Nd^{3+} site as mentioned before. This behaviour is common in multi-site materials as reported in the literature [11, 13]. These sites are at least one order of magnitude weaker than the others sites α, β, ε and ξ.

After some of different possible sites were identified, we recorded site-selective emission spectra as described in the experimental procedure of section 3. Figure 3 shows some emissions measured of sites α, β, γ, δ, ε, ξ and ζ when individual sites were excited in the main laser transition $^4F_{3/2}(R_1) \rightarrow {}^4I_{11/2}(Y_1, Y_2, \ldots, Y_6)$. However, many other recorded emission spectra, which have been omitted for the sake of brevity, show more than six emission bands because some excitation lines can excite more than one single site simultaneously, as shown in figure 2 for the sites β and ζ in the $^4F_{3/2}(R_1)$ domain. The emissions recorded on changing the excitation with small steps allowed us to identify different emission spectra; however, in some cases, on changing the excitation inside the same band $^4I_{9/2}(Z_1) \rightarrow {}^4F_{3/2}(R_1)$ we have obtained different emission spectra that confirm another site being present inside this

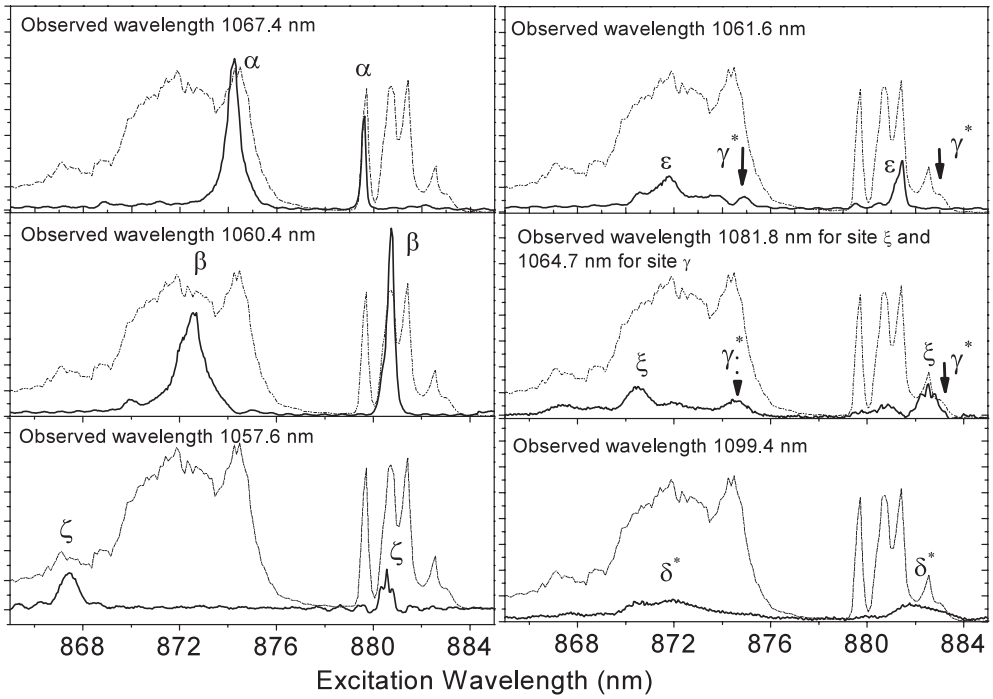

Figure 2. Site-selective excitation spectra of $NdNbO_4$-doped $CaMoO_4$ at 12 K. The small peak in 874.6 nm that appears above the excitation band of ξ and ε corresponds to a new site labelled as γ that was found by a site-selective emission experiment, and the sites marked with (*) mean the most probable positions of these sites.

band. This is for example the case of site δ and site γ, whose most probable positions were identified by this procedure, and after we selected one of the lines that was not coincident with the emission wavelength of another site we repeated the experiment of site-selective laser excitation, fixing the wavelength selected in the monochromator and recording the intensity of this line by changing the laser excitation. The difficulty found in this procedure is the overlap of excitation bands which makes the accurate characterization and separation of the $^4I_{11/2}$ Stark levels difficult. However, additional data analysis helps to elucidate how the Nd^{3+} and Nb^{5+} sites could be organized. Figure 4 summarizes all peak position wavelengths of emission obtained by all steps of wavelengths of excitation, represented by a cross symbol ($\times$), detected from the emission spectra as a function of the excitation wavelength for the transition $^4F_{3/2}(R_1) \rightarrow {}^4I_{11/2}(Y_1, Y_2, \ldots, Y_6)$. The marked positions were obtained using the criterion of maximum intensity as described to characterize other materials [10] that permits us to visualize all spectra simultaneously and separate each Stark component of the $^4I_{9/2}$ level. The black points ($\bullet$) indicate the positions of most intensity of the observed emission and excitation. The numbers in the graph indicate the six expected lines for $^4F_{3/2} \rightarrow {}^4I_{11/2}$ transitions $Y_1, Y_2, Y_3, \ldots, Y_6$, and the vertical lines indicate the most probable position of each site R_1 Stark level; this assertion was made by taking into account also the position of each site obtained by site-selective laser excitation bands of figure 2. The number of sites and the energy position bands also seems to agree with the number and energy obtained from the site-selective excitation spectrum of figure 2. However, some bands in $^4F_{3/2}(R_1)$ look larger than others (observed in figure 3 for the site α where six bands were expected and four bands observed).

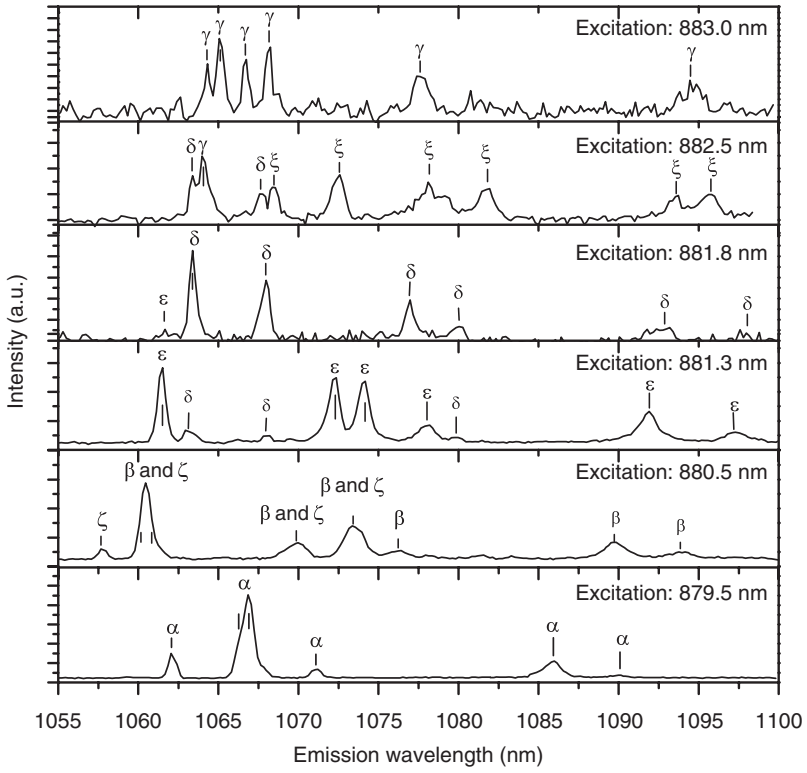

Figure 3. Some emission spectra at 15 K of Nd^{3+} sites in the spectral region of laser interest, $^4F_{3/2} \rightarrow {}^4I_{11/2}$ transitions for different wavelengths.

Table 1. Energy levels (cm^{-1}) of $^4F_{3/2}$ (R_1 and R_2) and $^4I_{11/2}$ ($Y_1, Y_2, \ldots, Y_6$) manifolds of each Nd^{3+} site in $NdNbO_4$-doped $CaMoO_4$. The value $(R_1 + R_2)/2$ indicates the gravity centre between R_1 and R_2 Stark levels. The sites δ and γ marked require more precise analysis.

Levels	Stark levels	α	β	ε	ξ	ζ	δ^*	γ^*
$^4F_{3/2}$	R_2	11 367.4	11 354.0	11 342.2	11 331.4	11 356.3	11 339.7	11 332.0
	$(R_1 + R_2)/2$	11 403.2	11 407.0	11 406.6	11 409.5	11 442.2	11 404.8	11 412.1
	R_1	11 439.0	11 460.0	11 471.0	11 487.6	11 528.2	11 469.9	11 492.3
$^4I_{11/2}$	Y_1	2 182.6	2 223.3	2 242.7	1 988.4	2 215.8	2 249.1	1 967.5
	Y_2	2 147.2	2 185.4	2 197.7	2 030.0	2 179.5	2 204.2	1 983.1
	Y_3	2 121.4	2 076.1	2 078.6	2 078.0	2 040.1	2 098.0	1 994.0
	Y_4	1 987.2	2 051.5	2 046.2	2 111.1	2 010.4	2 070.7	2 076.7
	Y_5	1 983.1	2 011.8	2 029.3	2 211.6	1 926.2	1 993.0	2 102.4
	Y_6	1 940.6	1 923.9	1 935.6	2 227.3	1 901.4	1 952.9	2 221.0

This behaviour could indicate the existence of more transitions inside this region, implying the existence of more Nd^{3+} sites or some local distortion in the site. The sites δ and γ present a much less intense emission than other sites, which could means a lower occupancy of Nd^{3+} in those sites; thus its concentration in $CaMoO_4$ samples is less than in sites α, β, ε and ξ.

Table 1 contains the values of energy found for each Stark level. These data allowed us to draw a partial diagram of the $^4F_{3/2}$ and $^4I_{11/2}$ levels. Figure 5 displays the crystal field scheme of $^4F_{3/2}$ and $^4I_{11/2}$ manifolds of Nd^{3+} ions into each of the sites. Particular splitting of energy

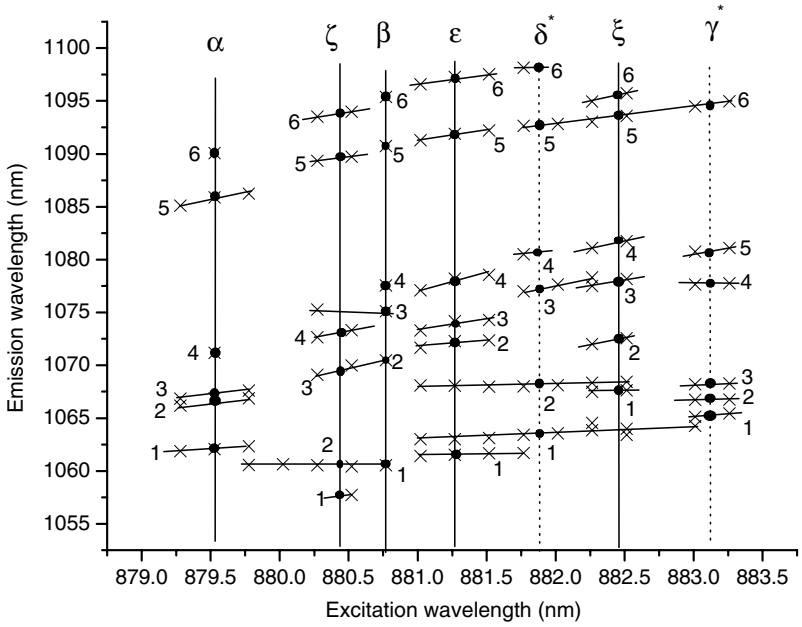

Figure 4. $^4F_{3/2}(R_1) \rightarrow {}^4I_{11/2}$ emission wavelength versus the excitation wavelength into the $^4F_{3/2}(R_1)$ doublet of $NdNbO_4$-doped $CaMoO_4$ at 15 K. Vertical lines are the most probable position of each site. The sites marked with (*) and with a dotted vertical line require a more precise analysis.

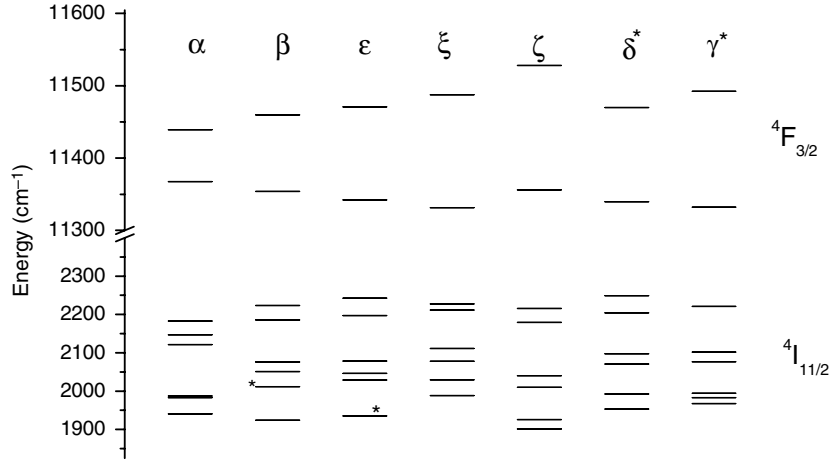

Figure 5. Energy level diagram corresponding to the $^4F_{3/2}$ (R_1 and R_2) and $^4I_{11/2}$ ($Y_1, Y_2, \ldots, Y_6$) manifolds of each Nd^{3+} site. The sites δ and γ and other levels marked (*) require more precise analysis.

between corresponding sites of $^4F_{3/2}(R_1)$ and $^4F_{3/2}(R_2)$ is observed. The magnitude of this splitting gives a rough estimation of the crystal field acting on the Nd^{3+} ions located at each site [8].

The features of the diagram of levels in figure 5 can be understood by a simplified model gathering the chemical nature and distribution of the participating cations in the crystal lattice,

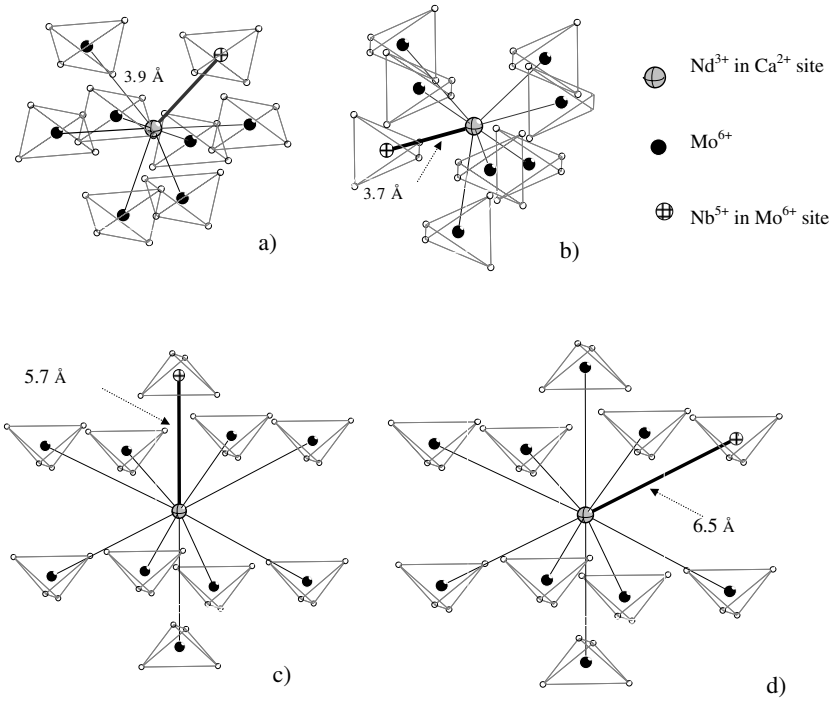

Figure 6. Possible configurations of $Nd^{3+}(Ca^{2+})$–$Nb^{5+}(Mo^{6+})$ complexes assigned as α, β, ε and ξ sites in $NdNbO_4$-doped $CaMoO_4$ at the first coordination sphere (a) and (b); at the second coordination sphere (c) and (d).

which should be discussed in terms of possible electroneutrality compensation mechanisms associated with the environment around each Nd^{3+} ion. The scheelite crystal structure is characterized by the tetragonal space group $I4_1/a$ or C^6_{4h} [12, 15]. Its structure has two primitive unit cells $CaMoO_4$. The calcium and molybdenum in this structure have a S_4 point symmetry, and the crystal has an inversion centre. The oxygen sites are arranged in approximately tetrahedral coordination about the molybdenum site [15]. In terms of the chemical neighbouring, the two constituent cations have eight-coordinated Ca^{2+} and four-coordinated tetrahedral Mo^{6+} sites [14]. According to the chemistry of solid-state reactions, after melting and solidification of the starting materials our crystals should have a composition close to $Ca_{1-x}Nd_xMo_{1-x}Nb_xO_{4-y}$ under ideal conditions. In such a formula, the existence of Nb^{5+} as charge compensator ion is expected, and the most favourable compensating charge defects are $Nd^{3+}(Ca^{2+})$–$Nb^{5+}(Mo^{6+})$ associations.

Figure 6 shows a close view of the chemical environment around Ca^{2+} and Mo^{6+} ions in $CaMoO_4$. Each Ca^{2+} ion lies in a dodecahedral site surrounded by neighbouring Mo^{6+} ions centred at oxygen tetrahedra [14–16]. This means a coordination number (CN) of 12 and 4 for Ca^{2+} and Mo^{6+} ions, respectively. The expected most favourable configuration of cation accommodation is that Nd^{3+} enters the Ca^{2+} sites and Nb^{5+} enters the Mo^{6+} sites because of their corresponding cationic radii, coordination numbers and valence state proximity. This configuration indicates that in such ideal situations there should be no more than four non-equivalent configurations of $Nd^{3+}(Ca^{2+})$–$Nb^{5+}(Mo^{6+})$ associations taking into account the closest Nd^{3+} neighbour cations. It is reasonable to assume that each configuration causes different perturbations or distortions in local symmetry around Nd^{3+}–O^{2-} dodecahedra that

modify the local crystal field, as indicated by the change in the energy splitting of sublevels in $^4F_{3/2}$ and $^4I_{11/2}$. Evidence of this can be noted in figure 5 for sites α, β, ε, and ξ, which show an increase in the splitting of energy with a slightly changed centre of gravity, while site ζ presents more intense splitting of energy and change of its gravity centre that indicates a decrease of Nd^{3+}–O^{2-} distances according to the nephelauxetic effect [13, 15]. The origin of even larger splitting could be attributed to Nd^{3+} occupation of the Mo^{6+} tetrahedral site, where Nd^{3+} would experience a more intense crystal field [6], forming a $Nd^{3+}(Mo^{6+})$–$Nb^{5+}(Ca^{2+})$ association with less probability to occur. Thus the large difference between the radius of the Nd^{3+} ion (0.98 Å for CN = 6, its value closer to CN = 4) and substituted Mo^{6+} ion (0.41 Å for CN = 4) should involve a considerable local distortion around this site. Moreover, additional distortion should occur around the Nb^{5+} ion (0.48 Å for CN = 4) and substituted Ca^{2+} (0.99 Å for CN = 12). Obviously, these distortions should be higher than that produced by $Nd^{3+}(Ca^{2+})$–$Nb^{5+}(Mo^{6+})$ associations [16].

Other possible configurations can be also proposed. Assuming that some oxygen vacancies could be present in the crystal along with residual $NdNbO_4$ according to the formulation $Ca_{1-x}Nd_{x-y}Mo_{1-x}Nb_{x-y}O_{4-y} + yNdNbO_4$, one can expect the possibility of many cation–$[O^{2-}]$ associations like $Nd^{3+}(Ca^{2+})$–$Nd^{3+}(Ca^{2+})$–$[O^{2-}]$ and several others related to vacancies and many kinds of colour centres (like F, F^+, F^-, F_2, F_3, F_4 or F_A) that have been observed by others authors [11, 18]. Such a situation could be the case for sites δ and γ that seem to have a large bandwidth in $^4F_{3/2}(R_1, R_2)$, as can be observed in figure 2. However, due to the low intensity of the excitation and emission spectra for these two sites, more experiments are necessary to characterize them accurately.

The observed emission spectra present different lifetimes changing the excitation spectra in the $^4F_{3/2} \rightarrow {}^4I_{11/2}$ transition, confirming the existence of multi-sites; however, due to the effect of overlap of excitation bands of most of these sites, the decay appears as non-exponential because of the contribution of the luminescence of each site. The average lifetime of this transition is 136 μs, and more information about the spectroscopy characteristics of this material can be found in the literature [3].

5. Conclusion

The analysis of our data has permitted us to identify clearly expected laser active sites and additional Nd^{3+} sites that have immediate effects on the energy diagram in $^4F_{3/2}$ and $^4I_{11/2}$ levels of Nd, Nb:$CaMoO_4$. Nd^{3+} active sites labelled α, β, ε and ξ should be related to $Nd^{3+}(Ca^{2+})$–$Nb^{5+}(Mo^{6+})$ associations with Nd^{3+} located at dodecahedral sites. Such sites are characterized by the more intense absorption spectra in our samples, which confirm their predominance as laser active sites like in other laser materials [4, 5, 17–19]. The site labelled ζ is related probably to Nd^{3+} in a Mo^{6+} site, thus in a tetrahedral site, where Nd^{3+} should be perturbed by a more intense crystal field. The others sites labelled δ and γ are attributed to other cationic associations with different charge compensating mechanisms that could not be largely investigated with the spectroscopic techniques used.

Acknowledgments

This work was partially supported by the Brazilian agencies FAPESP, CAPES and CNPq. The authors thank Dr D Reyes Ardila and the Crystal Growth Group of Universidade de São Paulo-São Carlos for the synthesis of the material.

References

[1] Faure N, Borel C, Couchaud M, Basset G, Templier R and Wyon C 1996 *Appl. Phys.* B **63** 593
[2] Mermilliod N, Romero R, Chartier I, Garapon C and Moncorgé R 1992 *IEEE J. Quantum Electron.* **28** 1179
[3] Andrade L H C, Reyes Ardila D, Barbosa L B, Andreeta J P, Siu Li M, Brenier A, Guyot Y and Boulon G 2005 *Eur. Phys. J. Appl. Phys.* **29** 55
[4] Ducan R C 1964 *J. Appl. Phys.* **36** 874
[5] Blistanov A A, Galagan B I, Denker B I, Ivleva L I, Osiko V V, Polozkov N M and Sverchkov Y E 1989 *Sov. J. Quantum Electron.* **19** 747
[6] Caldiño U, Voda G M, Garcia Solé J and Kaminskii A A 1993 *Chem. Phys. Lett.* **213** 84
[7] Caldiño U, Jaque G F, Balda R, Fernández J and Kaminskii A A 1995 *Opt. Mater.* **4** 713
[8] Guyot Y, Bausá L E, Camarillo E, Garcia Solé J, Vergara I, Monteil A and Moncorgé R 1992 *J. Appl. Phys.* **72** 5876
[9] Reyes Ardila D, Andreeta J P, Ribeiro C T M and Siu Li M 1999 *Rev. Sci. Instrum.* **70** 4606
[10] Burlot R, Moncorgé R and Boulon G 1997 *J. Lumin.* **72** 812
[11] Ermeneux F S, Goutaudier C, Moncorgé R, Cohen-Adad M T, Bettinelli M and Cavalli E 1999 *Opt. Mater.* **13** 193
[12] Hahn T (ed) 1987 *International Tables for Crystallography* vol A (Boston: Reidel)
[13] Garapon C, Lou L and Moncorgé R 1998 *J. Lumin.* **79** 161
[14] Hazen R M and Finger L W 1985 *J. Phys. Chem. Solids* **46** 253
[15] Zhang Y, Holzwarth N A W and Williams R T 1998 *Phys. Rev.* B **57** 12738
[16] Sleight A W 1972 *Acta Crystallogr.* B **28** 2899
[17] Gatterer K, Pucker G, Fritzer H P and Arafa S 1994 *J. Non-Cryst. Solids* **176** 237
[18] Tocho J O, Jaque F and Garcia Solé J 1992 *Appl. Phys. Lett.* **60** 3206
[19] Elouadi B, Powell R C and Holt S L 1987 *J. Solid State Chem.* **69** 369